Journal of Aerosol Science 114 (2017) 55–61

Contents lists available at ScienceDirect

Journal of Aerosol Science

journal homepage: www.elsevier.com/locate/jaerosci

Effects of shielding gas temperature and flow rate on the welding fume particle size distribution

V.I. Vishnyakov*, S.A. Kiro, M.V. Oprya, A.A. Ennan

Physical-Chemical Institute for Environmental and Human Protection, National Academy of Sciences of Ukraine, 3 Preobrazhenska st., Odessa 65082, Ukraine

ARTICLE INFO

Keywords:
Arc welding
Shielding gas
Welding fumes
Particle size distribution

ABSTRACT

The disperse composition of welding fume from gas metal arc welding with various shielding gas temperatures and flow rates is studied. The dependencies of bimodal particle size distribution on the shielding gas temperature in range of 300–600 K and flow rate in range of 6–12 Lpm are demonstrated. It is shown that the shielding gas temperature increase leads to condensed material between modes redistribution and to total integration of inhalable particles.

1. Introduction

The gas metal arc welding (GMAW) is widely used as a semi-automatic or automatic arc welding process for joining metals and alloys in many applications. During arc welding, high-temperature metal vapors are generated by evaporation from molten welding wire tip, droplets that are transferred from the wire tip to the weld pool, and the surface of the weld pool itself. A fraction of generated metal vapors is transported by convection from the arc region and cools rapidly as it mixes with shielded gas and ambient air creating the vapor-gas mixture. Metal nanoparticles are formed by nucleation and nuclei growth from metal vapors, they are oxidized and solidified, and are called the primary particles. Subsequently, these particles collide, coagulate and form the inhalable particles (secondary particles) with size up to micrometer, which ascend from the arc, and released in the form of the welding fume.

Welding fumes inhalation is a great occupational health problem. Biological activity of the formed particles depends on physicochemical parameters, such as particle size distribution, morphology, specific surface area and chemical composition. The welding fume particles' size gives them a high probability of being deposited in the respiratory bronchioles and lungs alveoli where rapid clearance mechanisms are not effective (Antonini, 2003; Clap & Owner, 1977). Therefore, the particle size distribution of welding fumes is an important factor in determining the hazard potential of the fumes because it is an indication of depth to which the particles may penetrate into the lungs and the number of particles retained therein. As shown by Zimmer and Biswas (2001), the particle size distribution of welding fumes is multimodal and dynamically changed with respect to time. The different particle size distribution modes have different chemical composition (Berlinger et al., 2011; Jenkins & Eagar, 2005; Oprya et al., 2012; Sowards, Ramirez, Dickinson, & Lippold, 2008; Worobiec et al., 2007) and morphology (Carpenter, Monaghan, & Norrish, 2008; Sanibondi, 2015; Sowards, Ramirez, Dickinson, & Lippold, 2010; Tashiro, Zeniya, Murphy, & Tanaka, 2013).

Investigations of GMAW show that welding process depends on shielding gas properties (Kolarik, Kovanda, Kolarikova, Vondrous, & Kopriva, 2013; Murphy, Tanaka, Tashiro, Sato, & Lowke, 2009; Rao, Liao, & Tsai, 2010); in particular, Ojima (2006) and Topham et al. (2012) demonstrate dependency of particle size distribution on shielding gas flow rate.

The objective of this study is to investigate the effect of shielding gas (CO_2) temperature and flow rate on disperse composition of welding fume generated by GMAW.

* Corresponding author.
E-mail addresses: dr.v.vishnyakov@gmail.com, eksvar@ukr.net (V.I. Vishnyakov).

http://dx.doi.org/10.1016/j.jaerosci.2017.09.010
Received 5 September 2017; Accepted 7 September 2017
Available online 09 September 2017

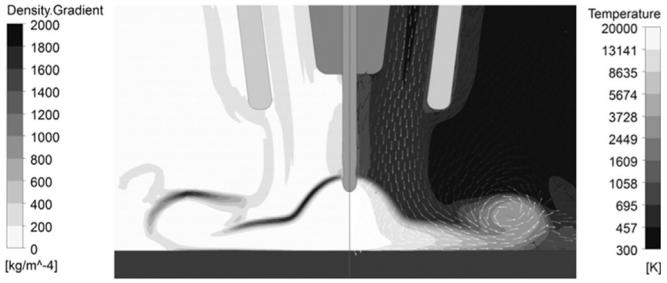

Fig. 1. Numerical simulation by Dreher et al. (2009).

2. Theoretical reasons for experiment

The high-temperature metal vapors from the weld materials mix up with shielding gas under the welding torch nozzle. As it follows from numerical simulation (Dreher, Füssel, & Schnick, 2009), which result is shown in Fig. 1, the gas average temperature in the boundary region at the torch outlet $T \sim 2500$ K. It means that nucleation occurs in the vapor-shielding gas mixture, before mixing with air.

The mass flow of vapor-gas mixture $J_{mix} = J_0 + J_{sg}$ is obtained by the turbulent mixing of the vapor mass flow J_0 with the shielding gas mass flow J_{sg}. The shielding gas flow rate can be approximately considered to be directly proportional to the mixture flow rate (Vishnyakov, Kiro, & Ennan, 2014b), i.e.

$$\frac{dJ_{sg}}{dt} = \frac{dJ_{mix}}{dt} = \alpha_T J_{mix},$$

where α_T is the factor, which is defined by the initial conditions of the vapors' efflux from the arc zone.

Hence, it follows,

$$J_{mix} = J_0 \exp(\alpha_T t), \quad J_{sg} = J_0[\exp(\alpha_T t) - 1]. \tag{1}$$

and the condensable components' mass fractions in the vapor-gas mixture are determined in the following form:

$$g_i(t) = \frac{g_{0i} J_0}{J_{mix}} = g_{0i} \exp(-\alpha_T t),$$

where g_{0i} is the initial component content in vapors.

Accordingly, the shielding gas mass fraction in mixture: $g_{sg} = 1 - \exp(-\alpha_T t)$, and the effective molecular mass of mixture is

$$\mu_{mix}(t) = \frac{1}{\sum g_i(t)/\mu_i + g_{sg}(t)/\mu_{sg}},$$

where μ_i is the components' molecular mass; μ_{sg} is the molecular mass of shielding gas (CO_2 in the case under consideration).

Thus, the current component partial pressure is described by equation:

$$P_i(t) = \frac{g_i(t)\mu_{mix}(t)}{\mu_i} P,$$

where P is the atmospheric pressure, and the number density of the component atoms is determined in the following form:

$$n_{Ai}(t) = \frac{g_i(t)\mu_{mix}(t)}{\mu_i} \frac{P}{k_B T(t)}. \tag{2}$$

Under assumption that a change in temperature of vapor-gas mixture occurs only by mixing with shielding gas, the current temperature can be described as:

$$T(t) = \frac{J_0 T_0 \sum (c_i g_{i0}) + J_{sg} T_{sg} c_{sg}}{J_0 \sum (c_i g_{i0}) + J_{sg} c_{sg}},$$

where T_0 is the initial vapor temperature; T_{sg} is the shielding gas temperature; c_i is the heat capacity of vapor component; c_{sg} is the heat capacity of shielding gas. Under assumption that $c_i = c_{sg}$, and with taken into account (1), the current temperature is determined in the following form:

$$T(t) = T_{sg} + (T_0 - T_{sg})\exp(-\alpha_T t). \tag{3}$$

From Eq. (3) follows:

$$\exp(-\alpha_T t) = \frac{T(t) - T_{sg}}{T_0 - T_{sg}},$$

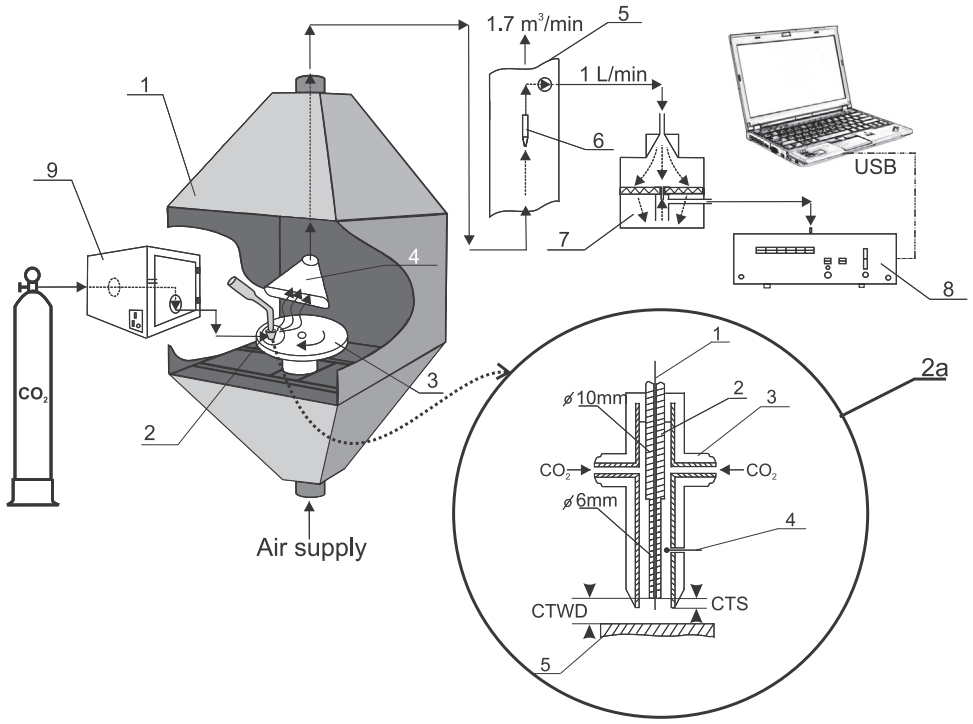

Fig. 2. Experimental equipment scheme: 1, fume chamber; 2, welding torch; 3, turntable; 4, slit air inlet; 5, vertical pipe; 6, nozzle for isokinetic sampling; 7, aerosol diluter; 8, laser aerosol spectrometer; 9, muffle electric furnace. a: Torch scheme: 1, electrode wire; 2, contact tube; 3, welding torch nozzle (internal diameter 15 mm) with thermal insulation; 4, thermocouple; 5, mild steel plate; CTWD is the contact tube to workpiece distance (9 mm); CTS is the contact tube setback (4 mm).

hence the number density of component atoms (2) can be determined as:

$$n_{Ai}(t) = \frac{P}{k_B T(t)} \cdot \frac{g_{i0}}{\mu_i \sum \frac{g_{i0}}{\mu_i} + \frac{\mu_i}{\mu_{sg}} \frac{T_0 - T(t)}{T(t) - T_{sg}}}. \tag{4}$$

Thus, the current number density of condensable atoms depends on the shielding gas temperature T_{sg} (namely, n_A decreases when T_{sg} increases), i.e. the shielding gas temperature must influence the nucleation and the nuclei condensation growth, and effect on welding fume particle disperse composition.

3. Experimental equipment and technique

The experimental equipment schematic diagram used for welding fume particle size distribution measurement is shown in Fig. 2. Welding fume was generated by the welding on rotated flat mild steel plates with thickness of 10 mm under the stationary torch inside the fume chamber. The DC MMA/TIG/MIG/MAG Paton PSI-250R invertor rectifier was used for producing welding fumes using ER 70S-6 welding wire with 0.8 mm diameter. The reverse polarity (i.e. electrode wire is positive and the plate is negative) direct current in the range of 85–100 A and voltage in the range of 18.5–21.5 V was used, as the manufacturer of the electrode wire recommends. Wire feed speed was determined by measuring the length of wire exiting the welding torch in a measured time. Average current over the test period is measured using a shunt connected to a moving coil meters. A constant contact tube to workpiece distance (9 mm) and the angle (90°) measured between the plate and the wire axis was maintained throughout all tests. Shielding gas (CO_2) flow rates in welding were measured using the rotameter in gas supply line and the temperature – by the thermocouple NMTXL-IM100-300 in the welding torch gas nozzle. Muffle electric furnace in gas supply line was used for the shielding gas heating during welding.

The welding fume plume was localized by extracting air at a distance of 20 cm from the welding arc with a flow of 1.7 m^3/min and redirected into the vertical pipe for isokinetic sampling of welding fume with flow rate of 1 Lpm (Oprya et al., 2012).

The welding fume dispersion was measured using the laser aerosol spectrometer LAS-P (LAS-P, 2010). The multichannel size distribution has the following optical latex-equivalent diameter ranges (μm): 0.15–0.2; 0.2–0.25; 0.25–0.3; 0.3–0.4; 0.4–0.5; 0.5–0.7; 0.7–1.0; 1.0–1.5; >1.5. The maximum relative error in determining the particle sizes and their number density is 5% and 10%, respectively, when the particle number density in a sample flow is less than $2 \cdot 10^3$ cm^{-3}.

The particle number density in the sample has the typical value of $\sim 10^5 cm^{-3}$. Therefore, the aerosol diluter with the dilution ratio of 150 for sample flow rate 1 Lpm was used (Fig. 2). Petryanov's filters with the collection efficiency of at least 99.97% for the particles with size of $0.15 - 0.2\mu m$ were used in the diluter.

The welding fume particle disperse composition is described by three-modal particle size distribution, that is determined experimentally (Ennan, Kiro, Oprya, & Vishnyakov, 2013) and described theoretically (Vishnyakov, Kiro, & Ennan, 2013, 2014a, 2014b; Vishnyakov, Kiro, Oprya, & Ennan, 2014), where the first two modes are the agglomerates of condensed primary particles and the third mode is coarse fume particles, formed by the disintegration of the electrode wire. Coarse particles with size larger than 1 μm are very few, and they do not affect the measured particle number densities for the first eight LAS-P channels. However, they make significant additives to the generated welding fume mass.

The best approximation for measurements in the range of 0.15 to 1 μm is the linear combination of two weighted lognormal distributions:

$$f(d, x, d_{m1}, \sigma_1, d_{m2}, \sigma_2) = x \cdot f_1(d, d_{m1}, \sigma_1) + (1 - x) \cdot f_2(d, d_{m2}, \sigma_2), \tag{5}$$

$$f_i(d, d_{mi}, \sigma_i) = \frac{1}{d\sqrt{2\pi}\ln\sigma_i} \exp\frac{-(\ln d - \ln d_{mi})^2}{2\ln^2\sigma_i},$$

where d_m is the median of distribution; σ is the standard deviation, x is the particle fraction in the first mode.

For each LAS-P channel j the following equation can be formulated

$$N_j = N_T \cdot \Delta d_j \cdot f(d_{cj}, x, d_{m1}, \sigma_1, d_{m2}, \sigma_2), \tag{6}$$

where N_j is the number of particles in the channel; N_T is the unknown total number of particles, which includes the particles with diameter $d < 0.15\,\mu$m; Δd_j is the channel width; d_{cj} is the average channel size.

Solving the system of Eq. (6) for all LAS-P channels allow to determine the parameters of welding fume particle size distribution (5) and obtain the average diameter of the particles $\overline{d} = d_m \exp(\ln^2\sigma/2)$ and their number densities for each of two modes: $n_1 = xn_T$, $n_2 = (1 - x)n_T$, where n_T is the total number density of the trapped particles.

4. Experimental results and discussion

The typical distributions of the measured particle number on the sizes are presented in Fig. 3 with approximation by Eq. (5).

The dependencies of the first two modes' average particle sizes on shielding gas temperature are presented in Fig. 4. Fig. 5 presents the similar dependencies of the particle number densities, and the fume generation rate (without taking coarse particles into account) is demonstrated in Fig. 6. The following weld parameters are used: the current $I = 90 \pm 5$ A; the voltage $U = 21 \pm 0.5$ V; the wire feed speed $v = 7 \pm 0.5$ cm/s; the shielding gas volumetric rate $Q = 10 \pm 0.1$ Lpm. These parameters provide the arc length of about 6 mm and drop spray transfer mode.

As it follows from Eq. (4), the number of condensable atoms is decreased while shielding gas temperature increases. Therefore, the total particle number density and total fume generation rate should also decrease under this condition, and it is demonstrated in Figs. 5 and 6.

The shielding gas temperature increase causes the decrease of mixture cooling rate, because from Eq. (3) follows:

$$\frac{dT}{dt} = -\alpha_T(T_0 - T_{sg})\exp(-\alpha_T t).$$

As shown by Shigeta, Watanabe, and Nishiyama (2004) and Shigeta and Murphy (2011), the cooling rate decrease results in particle sizes increase and particle number density decrease in the process of growth via vapor condensation. Therefore, the particle average size should be increased under shielding gas temperature increase, as is demonstrated in Fig. 4.

The total fume generation rate poorly decreases with the shielding gas temperature increase. At the same time, there is redistribution of condensed material between modes: the total material in the first mode decreases and in the second mode – increases with the shielding gas temperature increase.

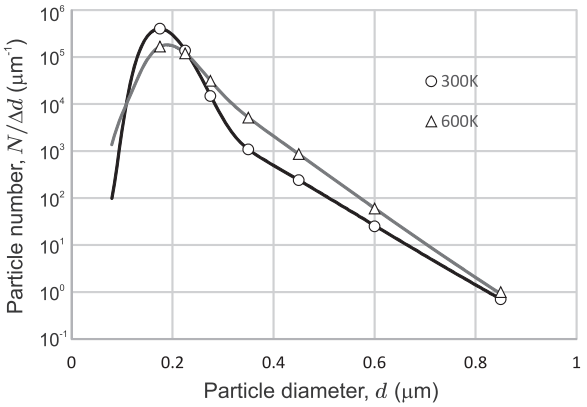

Fig. 3. Typical size distributions of the particle number N in relation to the channel width Δd (see Eq. (6)); curves are approximations by Eq. (5).

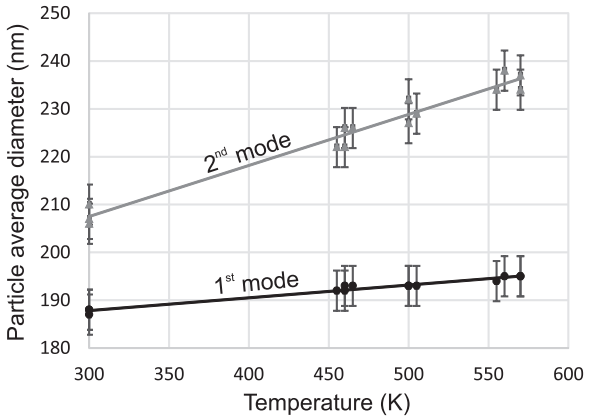

Fig. 4. Dependencies of average inhalable particle sizes on shielding gas temperature.

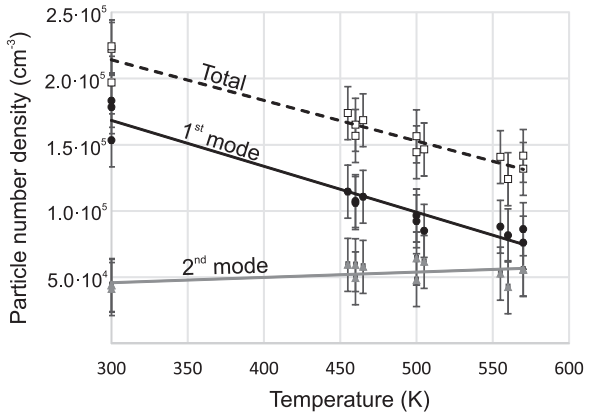

Fig. 5. Dependencies of inhalable particle number densities on shielding gas temperature.

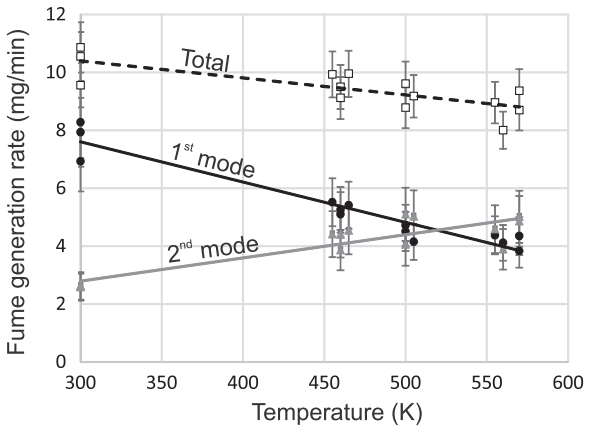

Fig. 6. Dependencies of fume generation rate on shielding gas temperature.

The dependencies of the first two modes' average particle sizes on the shielding gas volumetric flow rate are presented in Fig. 7. Similar dependencies of the particle number densities are presented in Fig. 8. In this case the following weld parameters are used: the current $I = 95 \pm 5$ A; the voltage $U = 20 \pm 0.5$ V; the wire feed speed $v = 8 \pm 0.5$ cm/s; the shielding gas temperature $T = 300$ K.

As it follows from presented results, the influence of shielding gas flow rate is in limits of the measurements error. These results differ from presented by Topham et al. (2012), where shielding gas (75% Ar and 25% CO_2) flow rate strongly effects on the particle sizes and number density. However, it should be noted that Topham et al. (2012) used the flow rate in the range of 20–30 Lpm, whereas in case under consideration the flow rate is 6–12 Lpm. Ojima (2006) demonstrates the relation between the fume concentration (mass density) in the breathing zone and the shielding gas flow rate in the range of 10–40 Lpm; where fume level is hardly

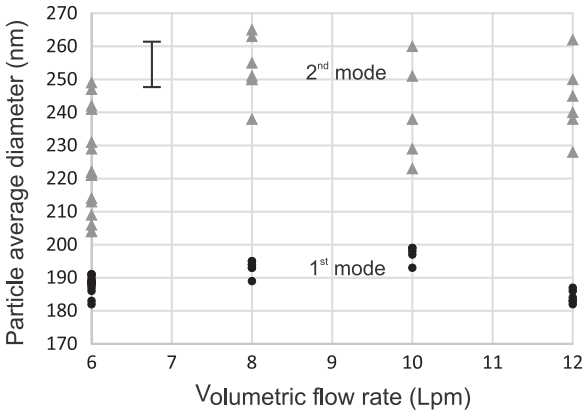

Fig. 7. Dependencies of particle average sizes on shielding gas flow rate.

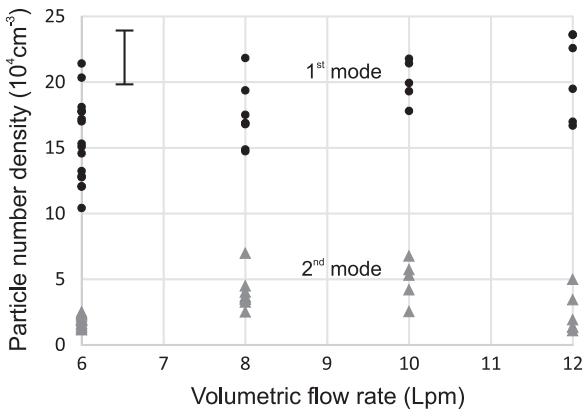

Fig. 8. Dependencies of particle number densities on shielding gas flow rate.

affected by the shielding gas flow rate, provided that the flow rate is less than 25 Lpm, and when the flow rate is over 25 Lpm, the fume concentration rapidly increased with increase of the flow rate.

5. Conclusion

The shielding gas flow rate in the range of 6–12 Lpm poorly influences the disperse composition of welding fume particles, whereas the shielding gas temperature provides essential impact.

The shielding gas temperature increasing causes the integration of both particle modes, which are formed in the processes of nucleation, nuclei growth and coagulation into inhalable particles. At the same time the total particle number density decreases with temperature increase.

The welding fume total generation rate poorly decreases with the shielding gas temperature increase. However, the intensive redistribution of the condensed material between modes occurs: the total material in the second mode increases with shielding gas temperature increase.

Thus, the shielding gas temperature increase leads to the integration of inhalable particles that should promote their more effective trapping by filters.

References

Antonini, J. M. (2003). Health effect of welding. *Critical Reviews of Toxicology, 33*(1), 61–103.

Berlinger, B., Benker, N., Weinbruch, S., L'Vov, B., Ebert, M., Koch, W., ... Thomassen, Y. (2011). Physicochemical characterisation of different welding aerosols. *Analytical and Bioanalytical Chemistry, 399*(5), 1773–1780.

Carpenter, K. R., Monaghan, B. J., & Norrish, J. (2008). Influence of shielding gas on fume size morphology and particle composition for gas metal arc welding. *The Iron and Steel Institute of Japan International, 48*, 1570–1576.

Clap, D. E., & Owner, R. J. (1977). An investigation of potential health hazard of arc welding fume growth with time. *Welding Journal, 56* (380s–385s).

Dreher, M., F¨ussel, U., Schnick, M., (2009). Simulation of shielding gas flowinside the torch and in the process region of GMA welding. Mathematical Modelling of Weld Phenomena (Technical University of Dresden), 9, 127–138.

Ennan, A. A., Kiro, S. A., Oprya, M. V., & Vishnyakov, V. I. (2013). Particle size distribution of welding fume and its dependency on conditions of shielded metal arc welding. *Journal of Aerosol Science, 64*, 103–110.

Kolarik, L., Kovanda, K., Kolarikova, M., Vondrous, P., & Kopriva, J. (2013). Influence of shielding gas on GMA welding of Al alloys. *Modern Machinery Science Journal,*

4, 452–455.
LAS-P (2010). *Laser Aerosol Spectrometer (LAS-P) model 9814.290.000.* Moscow: Karpov Institute of Physical Chemistry.
Murphy, A. B., Tanaka, M., Tashiro, S., Sato, T., & Lowke, J. J. (2009). Modelling of thermal plasmas for arc welding: the role of the shielding gas properties and of metal vapour. *Journal of Physics D: Applied Physics, 42* 194006.
Jenkins, N. T., & Eagar, T. W. (2005). Chemical analysis of welding fume particles. *Welding Journal, 84* (87s–93s).
Ojima, J. (2006). Performance of a fume-exhaust gun system in CO_2 arc welding. *Journal of Occupation Health, 48*, 207–209.
Oprya, M., Kiro, S., Worobiec, A., Horemans, B., Darchuk, L., Novakovic, V., ... Van Grieken, R. (2012). Size distribution and chemical properties of welding fumes of inhalable particles. *Journal of Aerosol Science, 45*, 50–57.
Rao, Z. H., Liao, S. M., & Tsai, H. L. (2010). Effects of shielding gas composition on arc plasma and metal transfer in gas metal arc welding. *Journal of Applied Physics, 107* 044902.
Sanibondi, P. (2015). Numerical investigation of the effects of iron oxidation reactions on the fume formation mechanism in arc welding. *Journal of Physics D: Applied Physics, 48* 345202.
Shigeta, M., Watanabe, T., & Nishiyama, H. (2004). Numerical investigation for nano-particle synthesis in an RF inductively coupled plasma. *Thin Solid Films, 457*, 192–200.
Shigeta, M., & Murphy, A. B. (2011). Thermal plasmas for nanofabrication. *Journal of Physics D: Applied Physics, 44*, 174025.
Sowards, J. W., Ramirez, A. J., Dickinson, D. W., & Lippold, J. C. (2008). Characterization of welding fume from SMAW electrodes - Part 1. *Welding Journal, 87* (106s-112s).
Sowards, J. W., Ramirez, A. J., Dickinson, D. W., & Lippold, J. C. (2010). Characterization of welding fume from SMAW electrodes - Part 2. *Welding Journal, 89* (82s–90s).
Tashiro, S., Zeniya, T., Murphy, A. B., & Tanaka, M. (2013). Visualization of fume formation process in arc welding with numerical simulation. *Surface and Coatings Technology, 228*, S301–S305.
Topham, N., Wang, J., Kalivoda, M., Huang, J., Yu, K.-M., Hsu, Y.-M., ... Paulson, K. (2012). Control of Cr^{6+} emission from gas metal arc welding using a silica precursor as a shielding gas additive. *The Annals of Occupational Hygiene, 56*(2), 233–241.
Vishnyakov, V. I., Kiro, S. A., & Ennan, A. A. (2013). Formation of primary particles in welding fume. *Journal of Aerosol Science, 58*, 9–16.
Vishnyakov, V. I., Kiro, S. A., & Ennan, A. A. (2014aa). Bimodal size distribution of primary particles in the plasma of welding fume: coalescence of nuclei. *Journal of Aerosol Science, 67*, 13–20.
Vishnyakov, V. I., Kiro, S. A., & Ennan, A. A. (2014bb). Multicomponent condensation in the plasma of welding fumes. *Journal of Aerosol Science, 74*, 1–10.
Vishnyakov, V. I., Kiro, S. A., Oprya, M. V., & Ennan, A. A. (2014c). Coagulation of charged particles in self-organizing thermal plasmas of welding fumes. *Journal of Aerosol Science, 76*, 138–147.
Worobiec, A., Stefaniak, E., Kiro, S., Oprya, M., Bekshaev, A., Spolnik, Z., ... Van Grieken, R. (2007). Comprehensive microanalytical study of welding aerosols with X-ray and Raman based method. *X-ray Spectrometry, 36*, 328–335.
Zimmer, A. T., & Biswas, P. (2001). Characterization of the aerosols resulting from arc welding processes. *Journal of Aerosol Science, 32*, 993–1008.